Distributed Converters in Large PV Plants: Performance Analysis Supported by Behavioral Models

Giovanni Nobile, Mario Cacciato, Giuseppe Scarcella, Giacomo Scelba, Ester Vasta, Agnese Giuseppa Federica Di Stefano, Giuseppe Leotta, Paola Maria Pugliatti, and Fabrizio Bizzarri

Abstract This paper is aimed to assess the performance of distributed converters in large PV plants through the analysis of a case study represented by a 2 MW PV plant in Central Italy. The electrical layout of a 500 kW subfield has been modified performing the installation of DC/DC converters at string level in order to create an independent MPPT control for every string. This kind of performance analysis is usually carried out using data acquired by the plant data logger. Unfortunately, the presence of partial unavailability, monitoring system faults, shutdown for maintenance activities, etc. can create several issues in data processing. To support data elaboration, a novel behavioral modeling approach has been developed and exploited in this work. This novel approach, based on an integrated state-space average model, can improve the performance analysis ensuring a satisfactory accuracy but keeping a low computation effort. Validation is performed considering real operating scenarios in case study.

1 Introduction

In large PV plants, the conversion system is usually realized using central inverters whose rated power is in the range from hundreds of kW to some MW. Such converters are usually installed into electrical cabins with fan cooling. The control system of central inverters often implements a single maximum power point tracking (MPPT) for the PV subfield connected to the DC bus of the inverter. In the literature, several papers deal with central inverters, and the research activities are focused mainly on converter topology [1], control system [2, 3], and modeling

G. Nobile (✉) · M. Cacciato · G. Scarcella · G. Scelba · E. Vasta
Department of Electrical, Electronics Engineering and Computer Science DIEEI, University of Catania, Catania, CT, Italy
e-mail: gnobile@dieei.unict.it

A. G. F. Di Stefano · G. Leotta · P. M. Pugliatti · F. Bizzarri
Enel Green Power SpA, Catania, Italy

W. Zamboni, G. Petrone (eds.), *ELECTRIMACS 2019*, Lecture Notes in Electrical Engineering 615, https://doi.org/10.1007/978-3-030-37161-6_42

[4]. On the contrary, there are no comprehensive analyses that investigate on distributed converters for large PV plants although their installation can provide significant benefits in terms of yield and reliability. Such benefits are related to the compensation of mismatch effects caused by nonuniform shadowing, faults in some PV modules, misaligned trackers, etc. [5]. In case of PV plants in operation from several years, distributed converters can limit the losses caused by the nonuniform aging of PV modules [6].

This work investigates on a specific distributed conversion typology represented by DC/DC converters in SiC technology installed at string level, close to the parallel string boxes. The case study is represented by a large PV plant in Central Italy. The layout of a subfield has been modified in August 2018 in order to allow the installation of such DC/DC converters. This paper reports the results of the experimental tests under different evaluation criteria. A novel integrated state-space average model has been developed and exploited with the purpose to replace wrong data occurring in case of faults in monitoring system, unavailability, missing data due to maintenance shutdown, etc.

The results shown in this paper can be effectively exploited in design process and in business planning of new PV plants as well as in retrofitting of existing fields.

2 Case Study

The case study of this work is represented by a ground-mounted 2 MW PV field in Central Italy, shown in Fig. 1. The plant is in operation since 2011. Technical data of the main components of the PV field are listed in Table 1. The rated power of PV modules is 235 W except for some strings in which 230 or 240 W PV modules have been used depending on their availability on the market during construction in 2011. The plant is divided into four subfields having similar rated power (about 500 kW). Each subfield is connected to a central inverter. There are two 1250 kVA transformers with double low-voltage windings each one fed by a central inverter.

This plant is chosen for the experimental tests because it is affected by nonuniform aging degradation in PV modules leading to relevant mismatch phenomena between strings. These phenomena, combined with local shadowing effects depending on the morphology of the terrain, have caused during the years significant differences between the subfields in terms of energy production.

With the purpose of reducing the gap between the yearly energy amount theoretically available and that really produced by the less performing 500 kW subfield (subfield 4), the string power optimizers in SiC technology have been installed in August 2018. Figure 2 shows some of the string optimizers during the assembly works on the rear side of the string boxes. As a consequence, the control system of the central inverter connected to the experimental subfield has been modified disabling the original MPPT control while regulating the DC link voltage value in a narrow range around 730 V. The obtained configuration for the experimental subfield is shown in Fig. 3, while Fig. 4 shows the standard power

Fig. 1 Pictures of the 2 MW PV plant in Central Italy that represents the case study of this work

Table 1 Technical specifications of the main power components in the 2 MW PV plant in Central Italy

PV modules (poly, 60 cells)	
P_{module}	235 W (230 or 240 in some strings)
V_{oc}	36.65 V (235 W module)
I_{sc}	8.59 A (235 W module)
V_{MPP}	28.70 V (235 W module)
I_{MPP}	8.19 A (235 W module)
P_{module}/T, V_{oc}/T, I_{sc}/T	−0.43%/°C, −0.35%/°C, +0.03%/°C
Strings and string boxes	
Modules in a string	20
Number of power inputs	16
Monitoring channels for string current	8 (the measured current is the sum of two strings)
String power optimizers	
Rated power	10 kW
Power inputs	1 PV array = 2 strings
Maximum efficiency	99.5%
Power device technology	SiC
Central inverters	
Number of inverters	4
Rated AC power	500 kVA
AC voltage, frequency	400 V, 50/60 Hz
MPPT DC voltage range	450–820 V
Maximum efficiency	98.6%

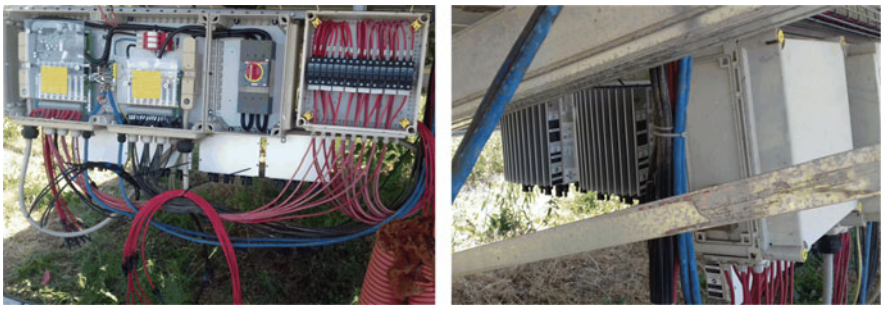

Fig. 2 Photos show the mounting of the string optimizers. Left: cabling modification at the string box. Right: string optimizers mounted at the rear side of the string box

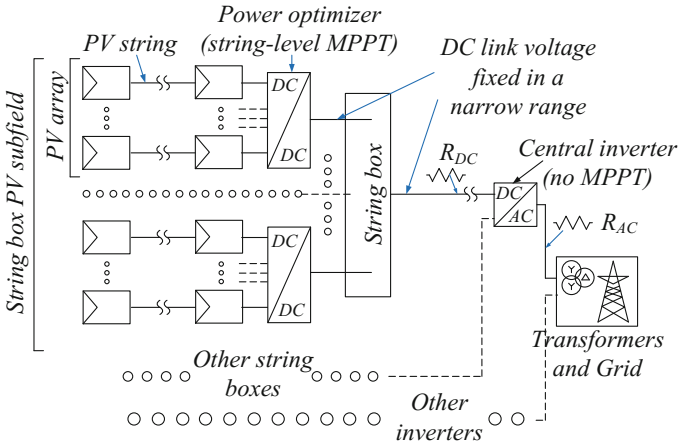

Fig. 3 Single line diagram of the experimental subfield whose original layout has been modified mounting the power optimizers at string level

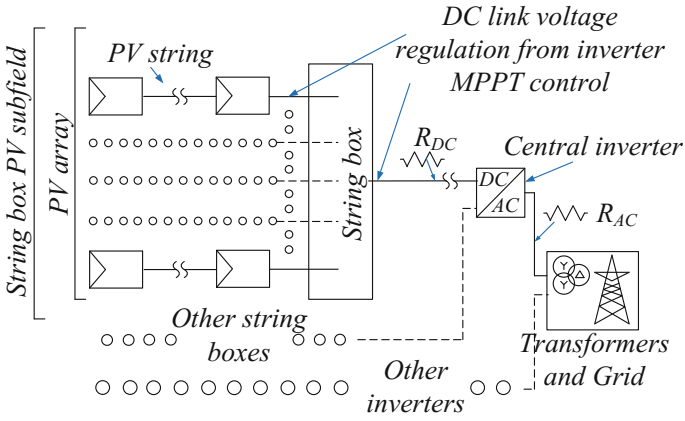

Fig. 4 Single line diagram of the subfields whose layout has maintained the original configuration

layout of the other three subfields (subfield 1, 2, 3) that have kept the original configuration. The monitoring system of the PV plant and of its subfields consists of several sensors and meters, whose accuracy can be assigned in the range from 1.5% to 2.5%.

3 Behavioral Modeling Approach

A suitable modeling approach, based on an integrated state-space average technique, has been developed to support data analysis for the performance assessment of distributed converters in large PV fields. Such behavioral model can be used to replace wrong or missing data in these cases:

- Faults in sensors and power analyzers
- Faults in monitoring system
- Partial or total unavailability due to electrical faults
- Shutdown of a subfield for maintenance activities
- Electrical quantities not provided by data loggers

Moreover, the model can compute all the electrical quantities in every section of the PV plant, thus allowing a simple calculation of losses, voltage drops, etc. On the contrary, in most real PV plant, the monitoring system does not provide all the electrical quantities for each section of the conversion system.

The basic general-purpose PV system configuration considered in this work is shown in Fig. 5. For both DC/DC converter and DC/AC conversion stage, it is possible to take into account simple topologies since the target is to build a behavioral model avoiding the complexity of the detailed models.

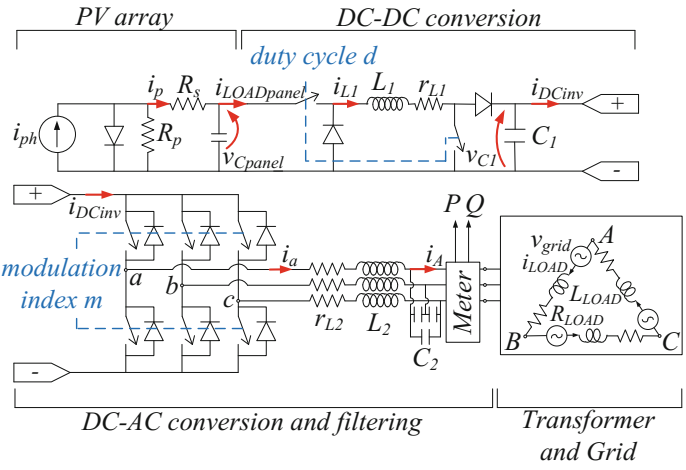

Fig. 5 Basic general-purpose configuration of a utility-scale PV field

3.1 Integrated State-Space Average Model

The integrated state-space average model used in this work is a modified version of the basic modeling approach presented by the authors in [7]. Such approach is a good trade-off between accuracy and computational complexity. The latter requirement is crucial in the performance assessment of utility-scale PV fields due to the large amount of data to be processed. Following the modeling approach described in [7], each component belonging to the conversion system of the PV plant in Fig. 5 has been modeled using its state-space average representation.

About the DC/DC converters, their model can be built as described in [8, 9] using the state-space average method. The implementation of the same method for DC/AC converters is usually performed in a different way, for example, using the symmetrical components as in [10]. In most cases, both the conversion stages are present in PV fields as for the case study. Unfortunately, the creation of an integrated model including all the conversion stages is difficult because of their different modeling approaches.

The key parameter to allow this matching is the DC link current i_{DClink}. Some authors have investigated the calculation of its average or RMS value exploiting power balances [11] or integration methods [12], in some cases with a reduced-order Fourier transform. The main drawback of these methods is the computational effort related to data storage in integrals. To overcome these issues, a novel calculation method has been developed obtaining a simple formula in which the average DC link current is a linear function of the symmetrical components of the AC currents:

$$\begin{aligned} i_{\mathrm{DCinv}} = (i_{\mathrm{DCinv}})_0 = \frac{\sqrt{3}m}{2} \Big[& x_1 \cos\left(\varphi_a - \tfrac{\pi}{6}\right) - x_2 \sin\left(\varphi_a - \tfrac{\pi}{6}\right) \\ & + x_3 \cos\left(\varphi_b - \tfrac{\pi}{6}\right) - x_4 \sin\left(\varphi_b - \tfrac{\pi}{6}\right) \\ & + x_5 \cos\left(\varphi_c - \tfrac{\pi}{6}\right) - x_1 \sin\left(\varphi_c - \tfrac{\pi}{6}\right) \Big] \end{aligned} \tag{1}$$

where $x_1, \ldots, x_6$ are the real and imaginary parts of the direct components of the virtual line AC currents:

$$\begin{aligned} (i_{ab})_1 &= x_1 + jx_2 \\ (i_{bc})_1 &= x_3 + jx_4 \\ (i_{ca})_1 &= x_5 + jx_6 \end{aligned} \tag{2}$$

and m is the modulation index of the inverter.

This result allows to integrate the models of converters belonging to multistage conversion systems. Moreover, a suitable procedure for obtaining the state-space models of the PV array, the filters, the transformer, and the grid and for merging all these models in a comprehensive representation of the whole PV plant is finally obtained, as it is reported in [7]. Using such approach, the PV plant is represented as a single state-space system whose inputs are the irradiance and module temperature and the outputs are the electrical quantities exploitable for loss evaluation and for

performance analysis. The analytical formulation of the final integrated state-space average model is in [7].

It is worth noting that, thanks to the adopted approach, technical details about the converters topology and their control system are no longer necessary. Since the state-space representation has a general validity, the proposed model can be implemented in any simulation platform.

3.2 Parameter Identification

The integrated state-space representation of the PV system allows the exploitation of several well-known identification methods in literature. Such methods can be also used to tune the regulator parameters in control systems. With the aim to implement an identification method with general validity for any plant configuration, a constrained minimum formulation can be applied in order to minimize the deviation between the model output and the real data collected by data loggers [13, 14]. To explain this method, let $y_{\text{measured}}(k)$ be an electrical variable acquired by the data logger in the form of a time series with N time samples:

$$[Y_{\text{measured}}] = \begin{bmatrix} y_{\text{measured}}(1) \\ y_{\text{measured}}(2) \\ \cdots\cdots\cdots\cdots \\ y_{\text{measured}}(k) \\ \cdots\cdots\cdots\cdots \\ y_{\text{measured}}(N) \end{bmatrix} \tag{3}$$

The corresponding quantity provided by the model is named $y_{\text{model}}(k)$. The latter can be considered the linear combination of the p_n parameters (unknown, to be identified) and of the terms h_{ki} that fix the relations between $y_{\text{model}}(k)$ and each p_i parameter:

$$y_{\text{model}}(k) = h_{k1}p_1 + h_{k2}p_2 + \cdots + h_{kn}p_n \tag{4}$$

For N time samples, this relationship becomes the following:

$$\begin{bmatrix} y_{\text{model}}(1) \\ y_{\text{model}}(2) \\ \cdots\cdots\cdots\cdots \\ y_{\text{model}}(k) \\ \cdots\cdots\cdots\cdots \\ y_{\text{model}}(N) \end{bmatrix} = \begin{bmatrix} h_{11} & h_{12} & \ldots & h_{1n} \\ h_{21} & h_{22} & \ldots & h_{2n} \\ \ldots & \ldots & \ldots\ldots & \\ h_{k1} & h_{k2} & \ldots & h_{kn} \\ \ldots & \ldots & \ldots\ldots & \\ h_{N1} & h_{N2} & \ldots & h_{Nn} \end{bmatrix} \begin{bmatrix} p_1 \\ p_2 \\ \ldots \\ p_n \end{bmatrix} \tag{5}$$

that is, in compact form:

$$[Y_{\text{model}}] = [H]\,[P] \tag{6}$$

Thanks to the constrained minimum formulation, the optimal set of parameters can be easily obtained as follows:

$$[P] \simeq \left([H]^T\,[H]\right)^{-1}[H]^T\,[Y_{\text{measured}}] \tag{7}$$

This formulation has been applied for each PV array in the experimental subfield, considering the rated power of the PV modules in each string (see Table 1).

4 Performance Analysis in Case Study

4.1 Implementation and Accuracy of the Behavioral Model

The usefulness of the proposed model can be pointed out with an example. Figure 6 shows the power curve of a PV array in the experimental subfield measured during a sunny day in the autumn 2018. The power waveform provided by the behavioral model is superimposed to the measured one. From 10:40 to 12:00, a maintenance shutdown occurs. Thanks to the model, it is possible to estimate with a good accuracy the theoretical energy during this shutdown. The relative error in the pink area ($\simeq$1.8%) is calculated from the following:

$$\varepsilon_{\%} = \frac{E_{\text{model}} - E_{\text{measured}}}{E_{\text{measured}}} 100 \tag{8}$$

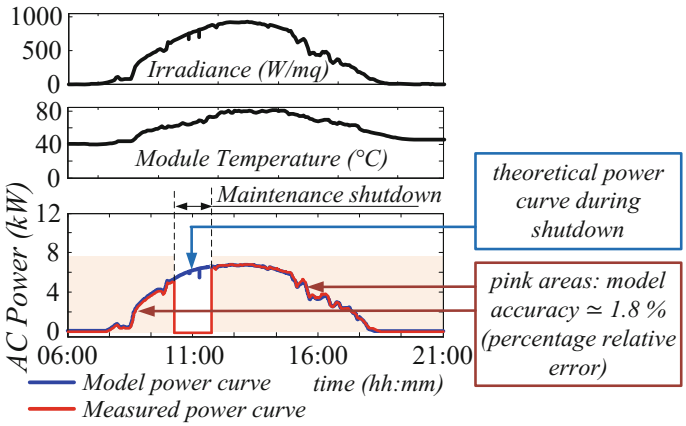

Fig. 6 Comparison between measured power and power curve provided by the behavioral model during a sunny day in autumn 2018. The behavioral model is used to trace the theoretical power curve during a maintenance shutdown

To establish an average reference value for the accuracy of the proposed modeling approach, the power curve provided by the model has been compared to the one measured in the field (at given irradiance and temperature) during several days in 2018 and 2019. The accuracy level calculated by Eq. (8) is in the range from 1.5% to 3.0% that is acceptable in comparison to the accuracy of standard power meters and sensors.

4.2 Execution Time Performance

The computational complexity of the behavioral model has been tested in comparison to the execution time of the detailed model referring to the basic PV system in Fig. 5 considering two different cases:

- Case A: The same simulation step size 1×10^{-6} s is assigned to the state-space average model and to the detailed one.
- Case B: A larger sample time equal to 2×10^{-5} s is assigned to the state-space average model. The step size of the detailed model is equal to the previous case; otherwise, such model cannot run properly.

For both cases, two different operating scenarios have been implemented and run 1000 times to get a large statistical database. The relative difference in execution times is summarized in Table 2. As expected, the behavioral model ensures a significant reduction in computational effort.

Table 2 Execution time performance evaluation, proposed vs. detailed model

	Case A, execution time	Case B, execution time
Scenario 1	Detailed model mean = 72.2 s, std = 3.0 s	Detailed model mean = 72.2 s, std = 3.0 s
	Proposed model, mean = 27.7 s, std = 4.8 s	Proposed model, mean = 3.5 s, std = 0.2 s
	Relative difference, mean = −61.6% std = 6.6%	Relative difference, mean = −95.1% std = 0.3%
Scenario 2	Detailed model mean = 72.1 s, std = 0.8 s	Detailed model mean = 72.1 s, std = 0.8 s
	Proposed model, mean = 30.0 s, std = 1.5 s	Proposed model, mean = 3.5 s, std = 0.1 s
	Relative difference, mean = −62.6% std = 2.2%	Relative difference, mean = −95.1% std = 0.1%

Simulation end time instant: 0.3 s. Scenario 1: 1000 W/m^2, 25 °C; scenario 2: 800 W/m^2, 45 °C; nonzero reactive power is forced after 0.1 s. Computer hardware: Intel Core i3-4005U CPU at 1.70 GHz (four CPUs), RAM 4096 MB, HD SSD 240 GB read speeds up to 545 MB/s, 64 bit

4.3 DC Cable Voltage Drops

In the experimental subfield, the measurement of the current in the cables that connect the optimizers and the DC link of the central inverter is not available. The cable is represented by its own resistance R_{DC} in Fig. 3. The integrated state-space average model described in this paper is able to calculate the average DC link current (flowing in DC cables) in a straightforward way as a linear function of the symmetrical components of the AC currents (see Sect. 3.1). In such a way, it is possible to evaluate in a direct way the actual voltage drop and Joule losses at each DC cable. Figure 7 shows some plots about the voltage drops in some DC lines of the PV plant. The behavioral model is used to replace data that are not provided by the monitoring system. Thanks to the higher DC voltage value, the voltage drop and the Joule losses are lower in the experimental subfield in comparison to the other subfields. However, in the PV plant under investigation, such effects can be neglected, thanks to the short lengths of DC cables and to their large cross sections.

5 Performance Analysis in Case Study

5.1 Daily PR of the PV Arrays in the Experimental Subfield

Figure 8 shows the distribution plots of the daily performance ratio (PR) for some PV arrays connected at the input of the DC/DC optimizers in the experimental subfields for the time periods:

- February 2018 to July 2018: "before" distributed converters (bDC period)
- August 2018 to February 2019: "after" distributed converters (aDC period)

The daily PR of each PV array is as follows:

$$\mathrm{PR}_{\mathrm{array}} = \frac{E_{\mathrm{array}}}{P_{\mathrm{array}}\mathrm{Rad}} \tag{9}$$

where P_{array} is the rated power of the array (sum of the rated power of two strings), Rad is the daily solar radiation, and E_{array} is the daily energy calculated from the power curve of the selected array. This power is calculated using the current value at the optimizer output and the DC link voltage; the latter also take into account the voltage drop on DC cables. Repeating the calculation in Eq. (9) for all the PV arrays in the experimental subfield and comparing bDC and aDC periods, the aggregate result in Fig. 9 shows that the average benefit obtained in terms of PR is about 2%.

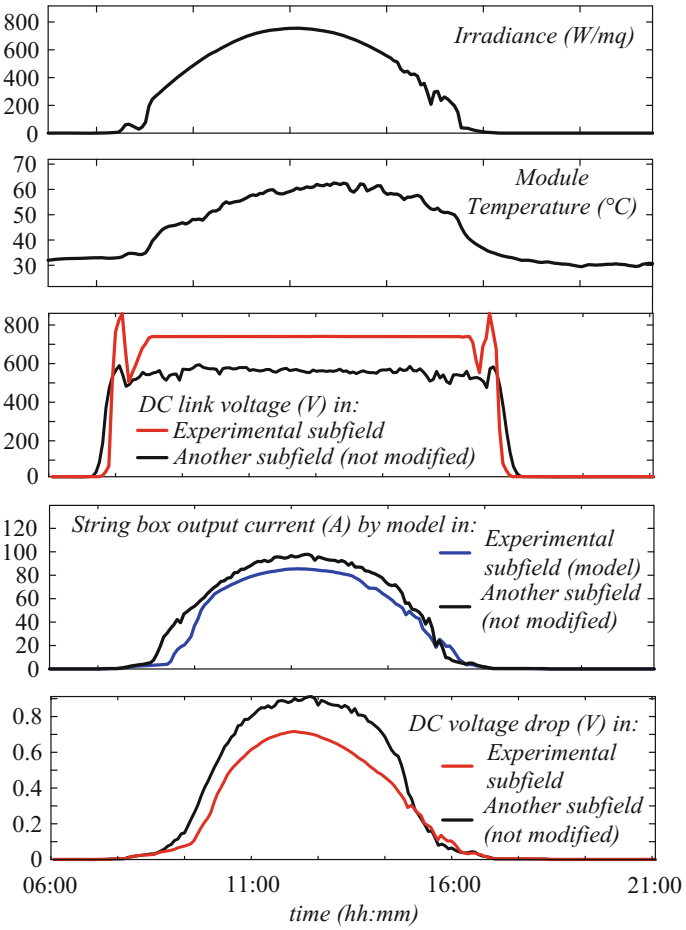

Fig. 7 Calculation of voltage drop during a sunny day in winter 2019. Comparison between the experimental subfield and another subfield with the original configuration

5.2 Central Inverter Operation

It is useful to investigate the behavior of the central inverter whose control system has been modified removing the original MPPT control and fixing the DC link voltage in a narrow range around 730 V. Figure 10 shows the main electrical quantities acquired by the data logger of the central inverter in the experimental subfield during 2 days belonging to the bDC and aDC period.

The following can be observed:

- The maximum efficiency in the aDC period is equal to the one measured in the bDC period (dashed line).

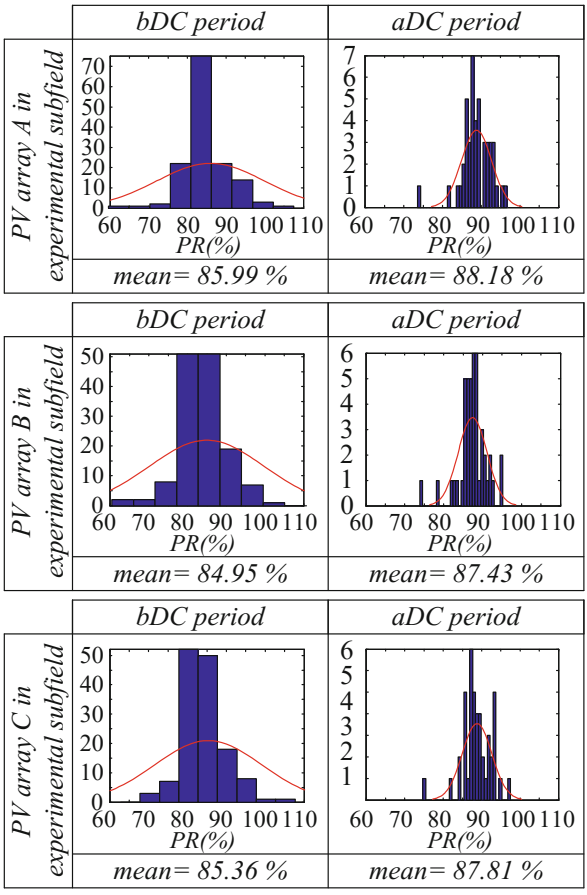

Fig. 8 (**a–c**) Distribution plots of the daily PR in some arrays of the experimental subfield for the periods bDC and aDC

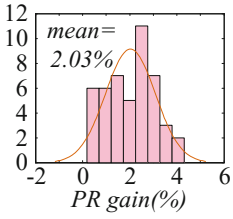

Fig. 9 Distribution plot of the PR gain in all the arrays of the experimental subfield, time period February 2018 to February 2019

- In the aDC period, during sunrise and sunset, the DC link voltage exhibits large fluctuations (yellow areas).
- The same phenomenon occurs in case of fast power variations (cyan areas) causing temporary significant decrease in efficiency level.

The modification of the control strategy in the central inverter implies bad effects on its operation in case of large power fluctuations, leading to a reduction in the energy gain measured at the AC side in variable weather conditions.

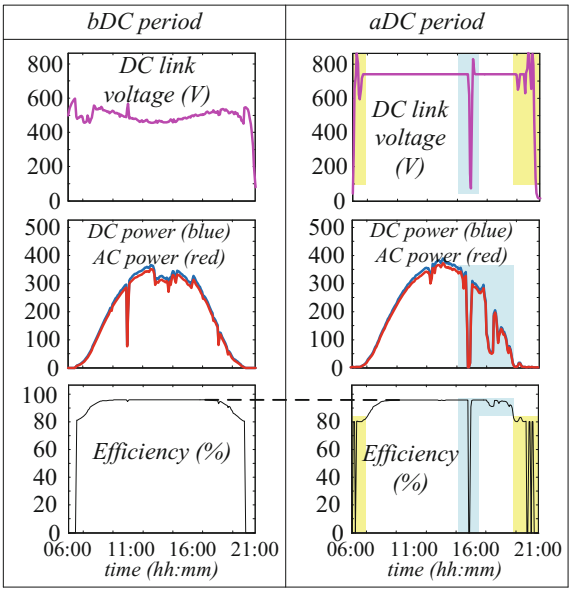

Fig. 10 Main electrical quantities acquired by the data logger of the central inverter in the experimental subfield during 2 days close to the installation date of the string optimizers

6 Conclusions

Although the performance assessment of large PV plants with distributed conversion systems is very topical, in literature, there is no a comprehensive overview on the available technical solutions. This paper contributes to fill this lack of information reporting the results coming from the performance evaluation of a large PV plant in Central Italy where DC/DC string optimizers have been mounted in a 500 kW experimental subfield. The average benefit in terms of PR at string level is about 2%. A suitable behavioral model has been developed and implemented to support the performance analysis in case of missing or wrong data. However, the operation of the inverter connected to string optimizers requires further investigations for future installations because of its impact on the energy recovery.

References

1. A. Cabrera-Tobar, E. Bullich-Massaguè, M. Aragues-Penalba, O. Gomis-Bellmunt, Topologies for large scale photovoltaic power plant. Renew. Sustain. Energy Rev. **59**, 309–319 (2016)
2. K. Zeb, W. Uddin, M.A. Khan, Z. Ali, M.U. Ali, N. Christofides, H.J. Kim, A comprehensive review on inverter topologies and control strategies for grid connected photovoltaic system. Renew. Sustain. Energy Rev. **94**, 1120–1141 (2018)
3. M. Cacciato, A. Consoli, New regenerative active snubber circuit for ZVS phase shift Full Bridge converter, in *IEEE Applied Power Electronics Conference and Exposition*, (IEEE, Piscataway, NJ, 2011), pp. 1507–1511

4. P. Han, Z. Lin, L. Wang, G. Fan, X. Zhang, A survey on equivalence modeling for large-scale photovoltaic power plants. Energies **11**, 1–14 (2018)
5. N. Agarwal, A. Agarwal, Mismatch losses in solar photovoltaic array and reduction techniques. MIT Int. J. Elect. Instr. Eng. **4**, 16–19 (2014)
6. P. Manganiello, M. Balato, M. Vitelli, A survey on mismatching and aging of PV modules: the closed loop. IEEE Trans. Indust. Elect. **62**, 7276–7286 (2015)
7. G. Nobile, M. Cacciato, G. Scarcella, G. Scelba, A.G.F. Di Stefano, G. Leotta, P.M. Pugliatti, F. Bizzarri, Comparison between central and string inverters performance for the utility-scale PV plant in Nova Olinda Brazil, in *35th European Photovoltaic Solar Energy Conference and Exhibition EU PVSEC*, (WIP, Munich, 2018), pp. 1935–1941
8. R.H.G. Tan, L.Y.H. Hoo, DC-DC converter modeling and simulation using state-space approach, in *IEEE Conference on Energy Conversion CENCON*, (IEEE, Piscataway, NJ, 2015), pp. 42–47
9. G. Kanimozhi, J. Meenakshi, V. Sreedevi, Small signal modeling of a DC-DC type double boost converter integrated with SEPIC converter using state space averaging approach. Energy Procedia **117**, 835–846 (2017)
10. Z. Lin, H. Ma, Modeling and analysis of three-phase inverter based on generalized state space averaging method, in *39th Annual Conference of the IEEE Industrial Electronics Society IECON*, (IEEE, Piscataway, NJ, 2013), pp. 1007–1012
11. J.W. Kolar, S.D. Round, Analytical calculation of the RMS current stress on the DC-link capacitor of voltage-PWM converter systems. IEEE Proc. Elect. Power Appl. **153**, 535–543 (2006)
12. X. Pei, W. Zhou, Y. Kang, Analysis and calculation of DC-link current and voltage ripples for three-phase inverter with unbalanced load. IEEE Trans. Power Electron. **30**, 5401–5412 (2015)
13. M. Galad, P. Spanik, M. Cacciato, G. Nobile, Comparison of common and combined state of charge estimation methods for VRLA batteries, in *ELEKTRO Conference*, (IEEE, Piscataway, NJ, 2016), pp. 220–225
14. G. Nobile, M. Cacciato, G. Scarcella, G. Scelba, Performance assessment of equivalent-circuit models for electrochemical energy storage systems, in *43rd Annual Conference of the IEEE Industrial Electronics Society IECON*, (IEEE, Piscataway, NJ, 2017), pp. 2799–2806. Chapter 46